Short Article

Molecular Cell

Physiological hypoxia restrains the senescence-associated secretory phenotype via AMPK-mediated mTOR suppression

Graphical abstract

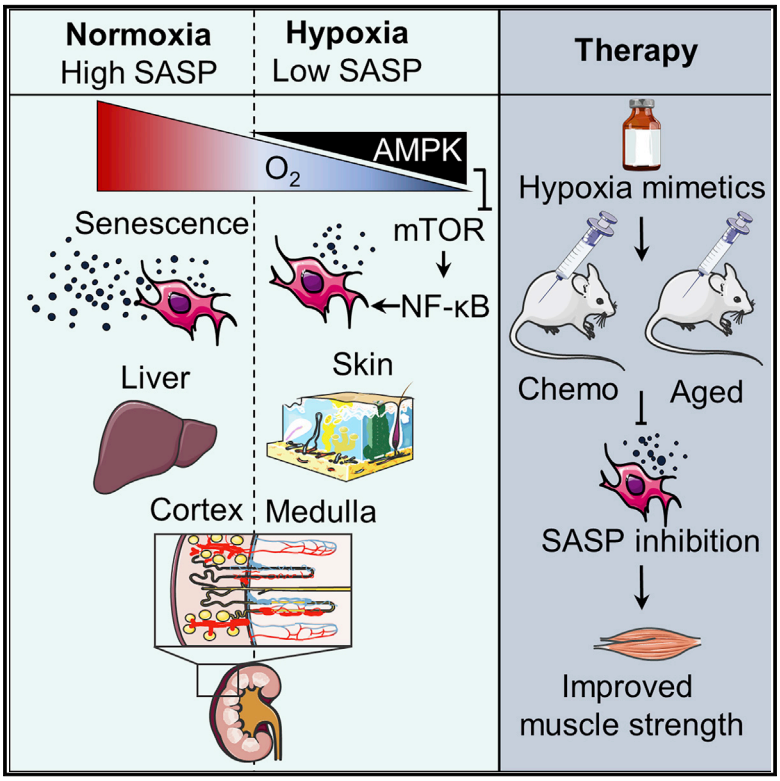

Highlights

- Physiologically hypoxic conditions restrain production of pro-inflammatory SASP
- Hypoxia blocks SASP production via suppression of the mTOR-NF-κB signaling loop
- Hypoxia-mimetic compounds limit SASP and improve strength in mice

Authors

Thijmen van Vliet, Marta Varela-Eirin, Boshi Wang, ..., Marc Seelen, Vassilis Gorgoulis, Marco Demaria

Correspondence

m.demaria@umcg.nl

In brief

Senescent cells secrete detrimental pro-inflammatory SASP factors that promote age-related dysfunctions and chemotoxicity. Van Vliet et al. show that the expression of pro-inflammatory SASP factors is significantly reduced in physiologically hypoxic conditions and that treatment with hypoxia mimetics reduces SASP and increases the health of aged and chemotherapy-treated mice.

van Vliet et al., 2021, Molecular Cell *81*, 2041–2052
May 6, 2021
https://doi.org/10.1016/j.molcel.2021.03.018

CellPress

Molecular Cell

CellPress

Short Article

Physiological hypoxia restrains the senescence-associated secretory phenotype via AMPK-mediated mTOR suppression

Thijmen van Vliet,[1] Marta Varela-Eirin,[1,7] Boshi Wang,[1,7] Michela Borghesan,[1] Simone M. Brandenburg,[1] Rossana Franzin,[2] Konstantinos Evangelou,[3] Marc Seelen,[2] Vassilis Gorgoulis,[3,4,5,6] and Marco Demaria[1,8,*]

[1]European Research Institute for the Biology of Ageing (ERIBA), University Medical Center Groningen, Groningen, 9713 AV, the Netherlands
[2]Experimental Nephrology Department, University Medical Center Groningen, University of Groningen, Groningen, 9713 GZ, the Netherlands
[3]Molecular Carcinogenesis Group, Department of Histology and Embryology, Medical School, National and Kapodistrian University of Athens, Athens 157 72, Greece
[4]Faculty Institute for Cancer Sciences, Manchester Academic Health Sciences Centre, University of Manchester, Manchester M13 9NQ, UK
[5]Biomedical Research Foundation, Academy of Athens, Athens 115 27, Greece
[6]Center for New Biotechnologies and Precision Medicine, Medical School, National and Kapodistrian University of Athens, Athens 157 72, Greece
[7]These authors contributed equally
[8]Lead contact
*Correspondence: m.demaria@umcg.nl
https://doi.org/10.1016/j.molcel.2021.03.018

SUMMARY

Cellular senescence is a state of stable proliferative arrest triggered by damaging signals. Senescent cells persist during aging and promote age-related pathologies via the pro-inflammatory senescence-associated secretory phenotype (SASP), whose regulation depends on environmental factors. *In vivo*, a major environmental variable is oxygenation, which varies among and within tissues. Here, we demonstrate that senescent cells express lower levels of detrimental pro-inflammatory SASP factors in physiologically hypoxic environments, as measured in culture and in tissues. Mechanistically, exposure of senescent cells to low-oxygen conditions leads to AMPK activation and AMPK-mediated suppression of the mTOR-NF-κB signaling loop. Finally, we demonstrate that treatment with hypoxia-mimetic compounds reduces SASP in cells and tissues and improves strength in chemotherapy-treated and aged mice. Our findings highlight the importance of oxygen as a determinant for pro-inflammatory SASP expression and offer a potential new strategy to reduce detrimental paracrine effects of senescent cells.

INTRODUCTION

Accumulation of irreparable cellular damage leads to senescence, a tumor-suppressive state of stable cell-cycle arrest caused by the upregulation of cyclin-dependent kinase inhibitors (CDKi) p21 and p16. Senescent cells show enlarged morphology, nuclear and chromatin remodeling, high lysosomal activity, resistance to apoptotic stimuli, and a complex transcriptionally regulated secretory program, collectively named the senescence-associated secretory phenotype (SASP) (Gorgoulis et al., 2019). The SASP includes a variable collection of cytokines, chemokines, proteases, and growth factors (Coppé et al., 2010; Hernandez-Segura et al., 2018b). NF-κB is arguably the major regulator of pro-inflammatory SASP factors in cells induced to senescence by DNA-damaging agents, but the composition and biological functions of the SASP remain highly heterogeneous and dependent on additional (epi-)genetic and environmental clues (Hernandez-Segura et al., 2018b). SASP factors regulate development and tissue regeneration and repair during both embryogenesis and adulthood (Demaria et al., 2014; Muñoz-Espín et al., 2013; Ritschka et al., 2017; Storer et al., 2013) but also contribute to tissue deterioration and chronic inflammation, eventually supporting the progression of age-related dysfunctions (Baker et al., 2016). Interventions that selectively eliminate senescent cells (senolytics) or modulate the SASP (senostatics or senomorphics) improve health span and reduce frailty (Xu et al., 2015, 2018; Yousefzadeh et al., 2018).

Oxygen partial pressure (pO_2) varies between and within organs as a consequence of tissue structure and availability of arterioles and capillaries. The mean tissue pO_2, also defined average normoxia, is ~40 mm Hg (~5% of air gases), but this tension can swing from 8 to 100 mm Hg (1%–12%) (Ast and Mootha, 2019; Ortiz-Prado et al., 2019). Mammalian cells have evolved programmed responses to oxygen concentrations and can quickly adapt to changes in oxygen levels by adopting different metabolic pathways. In low-oxygen conditions (also defined as hypoxia), cells reduce their energy expenditure by engaging the AMP-activated protein kinase (AMPK) signaling pathway and suppressing mammalian target of rapamycin (mTOR) activity (Brugarolas et al., 2004; González et al., 2020), switching from

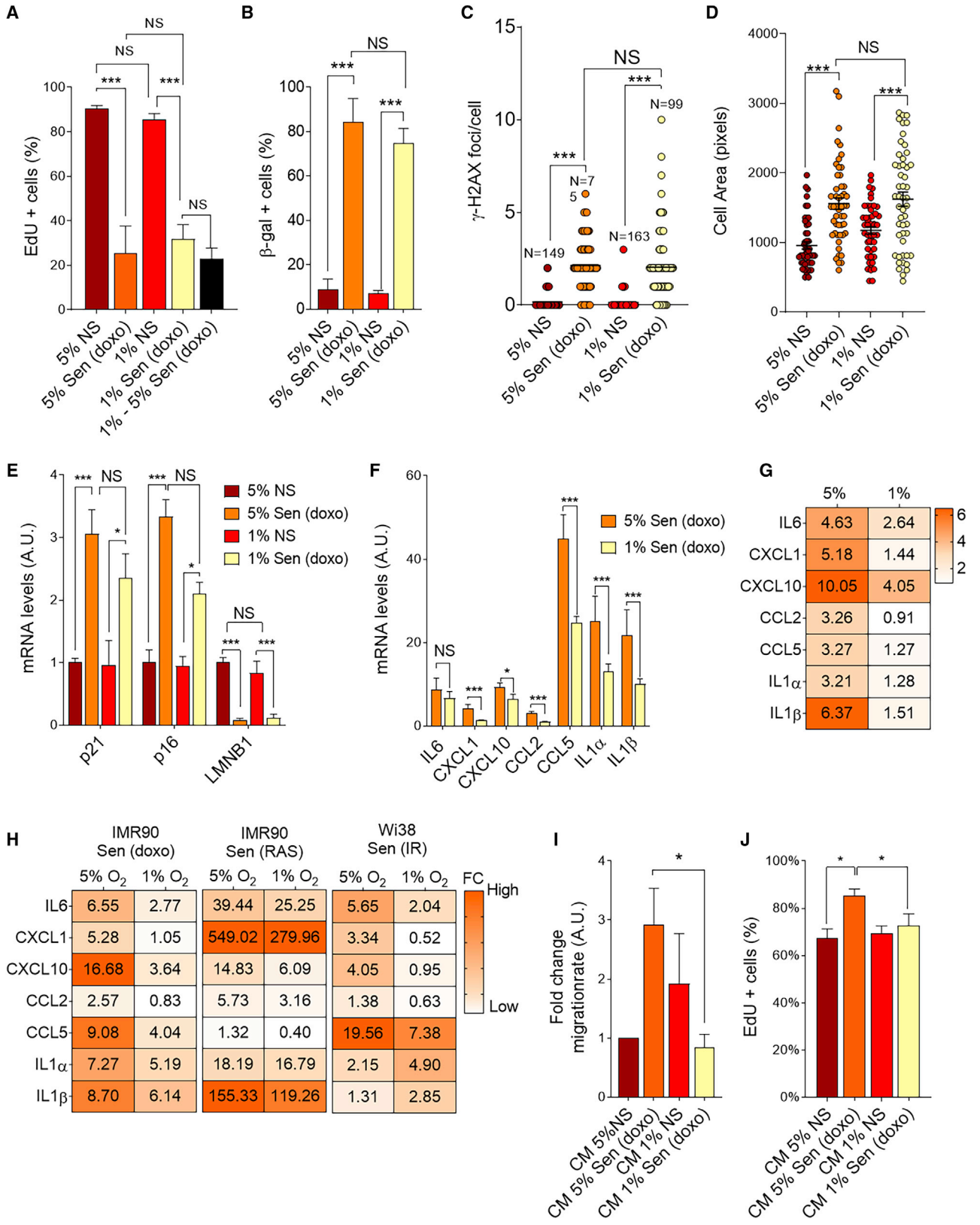

(legend on next page)

oxidative phosphorylation to glycolysis, and stimulating angiogenesis (Wenger, 2002).

Oxygen levels have a significant effect on senescence induction. Cellular cultures are mostly performed in a 95% air (79% N_2/21% O_2) atmosphere, supplemented by 5% carbon dioxide, thus providing 19.95% O_2. Under these hyperoxic conditions, the replicative lifespan of primary human and mouse fibroblasts is affected and senescence prematurely induced, mainly because of the excessive chronic oxidative stress at which cells are exposed (Casciaro et al., 2020; Parrinello et al., 2003; Chen et al., 1995). Moreover, mouse cells are unable to develop a robust SASP when cultured under atmospheric oxygen (Coppé et al., 2010). Hypoxia-like responses delay various types of premature senescence in cells cultured in normoxia (Welford et al., 2006; Kilic Eren and Tabor, 2014; Leontieva et al., 2012), while extreme hypoxia (0.2%) can prevent senescence induction by maintaining stressed cells in a quiescent state via repression of mTOR (Leontieva et al., 2012; Blagosklonny, 2014). Importantly, mTOR acts as a positive SASP regulator (Laberge et al., 2015; Herranz et al., 2015). However, data on the regulation of senescence-associated phenotypes in physiological hypoxia are missing. Here, we set to study how physiological hypoxia and hypoxia-mimetic compounds modulate the development of various senescence-associated phenotypes in culture and *in vivo*.

RESULTS

Hypoxia restrains the SASP in primary cultures

We initially treated primary human skin fibroblasts (BJ) with the genotoxic agent doxorubicin (doxo) and cultured cells at 1% (hypoxia) or 5% (normoxia) O_2. Successful activation of a hypoxia response in cells at 1% O_2 was demonstrated by enhanced expression of the glycolytic markers GLUT1 and PDK1 (Figure S1A). Hypoxic and normoxic doxo-treated cells equally lost proliferative capacity, as demonstrated by a steep reduction in EdU incorporation (Figure 1A; Figure S1B), while hypoxic and normoxic non-senescent cells maintained similar growth rates (Figure 1A; Figure S1B). Hypoxic doxo-treated BJs were unable to restore proliferation even when cells were switched back to normoxia (Figure 1A), suggesting that physiological hypoxia favors induction of senescence over the occurrence of a reversible and quiescence-like state, a phenomenon observed in cells exposed to genotoxic stress under conditions of severe hypoxia (0.2% O_2) (Leontieva et al., 2012). In accordance with the acquisition of a senescent phenotype, doxo-treated hypoxic cells developed various senescence-associated features, including enhanced senescence-associated β galactosidase (SA-βgal) activity, persistent DNA damage response (DDR), and enlarged morphology, with no significant differences with cells cultured in normoxic conditions (Figures 1B–1D; Figures S1C and S1D). mRNA levels of the CDKi p16 and p21, and of the nuclear lamina protein LaminB1, were equally up- and downregulated, respectively, in doxo-treated cells at 1% and 5% O_2 (Figure 1E). p16 protein levels demonstrated no differences due to oxygen concentration (Figures S1E and S1F). In contrast, hypoxic doxo-treated BJ cells expressed lower levels of mRNAs encoding for the pro-inflammatory SASP factors IL-6, CXCL1, CXCL10, CCL2, CCL5, IL-1α, and IL-1β in comparison with normoxic oxygen conditions (Figure 1F) and reduced secretion of the same factors in the conditioned medium (CM) (Figure 1G). Hypoxic primary lung fibroblasts (IMR-90) treated with doxo or transduced with RAS oncogene (RASVal12), and primary lung fibroblasts (WI-38) or renal proximal tubular epithelial cells (PTECs) exposed to ionizing γ-radiation (IR) similarly entered a state of stable growth arrest and induced SA-βgal activity but failed to mount a robust SASP (Figure 1H; Figures S1G–S1J). SASP factors can promote tumor cell migration and proliferation (Demaria et al., 2017; Sun et al., 2012; Murali et al., 2018). CM collected from normoxic BJ cells treated with doxo or WI-38 cells treated with IR accelerated migration and proliferation of the triple-negative breast carcinoma cells MDA-231 (Figures 1I and 1J; Figures S1K–S1M). In contrast, no effect was observed when MDA-231 cells were exposed to the CM collected from hypoxic senescent cells (Figures 1I and 1J; Figures S1K–S1M). Taken together, these data suggest that low-oxygen conditions reduce the activation and establishment of a pro-inflammatory and pro-tumorigenic SASP without affecting other senescence-associated features.

Tissue regions exposed to low oxygen accumulate senescent cells with negligible SASP

We then evaluated SASP expression in tissues and tissue regions that are physiologically exposed to different oxygen

Figure 1. Primary cells enter a senescent state with reduced SASP in hypoxia

(A–G) Human skin fibroblasts (BJ) were treated for 24 h with 250 nM doxorubicin (doxo) and cultured in 5% or 1% O_2 for 14 days. Proliferating cells treated with vehicle were used as non-senescent control cells (NS) (A). Cells were re-plated, incubated for 24 h with EdU, fixed, and stained. n = 9 from three independent experiments. (B) Cells were fixed and stained for SA-βgal. n = 9 from three independent experiments. (C) Cells were fixed and stained with an antibody against γH2AX. Number of foci per cell were quantified. Number of cells scored per each condition is indicated. (D) Cells were trypsinized, and the diameters of detached cells were measured using bright-field images of 50 cells per group. (E and F) Total RNA was extracted and the mRNA of the indicated genes quantified using qRT-PCR relative to housekeeping mRNA levels (mean actin/tubulin). n = 9 from three independent experiments. (G) Protein levels in the conditioned medium (CM) were measured using multiplex ELISA. n = 6 from three independent experiments.

(H) Total RNA was isolated from indicated cells and treatments, and mRNA levels of indicated genes were quantified using qRT-PCR relative to housekeeping mRNA levels (mean actin/tubulin). Fold changes (FCs) in mRNA levels were calculated using mRNA levels from non-senescent cells cultured in 5% O_2 as baseline. n = 9 from three independent experiments.

(I) Migration of MDA-231 cells exposed to CM from doxo-treated or control (ctrl) BJ cells was measured using transwells. n = 9 from three independent experiments.

(J) MDA-231 cells were exposed to conditioned medium (CM) from doxo-treated or non-senescent cells (NS) in the presence of EdU. Then, cells were fixed and stained. n = 9 from three independent experiments.

In (A)–(F), (I), and (J), two-tailed t test, *p < 0.05, **p < 0.01, and ***p < 0.001; NS, not significant. A.U., arbitrary units. Data are shown as mean ± SEM. See also Figure S1.

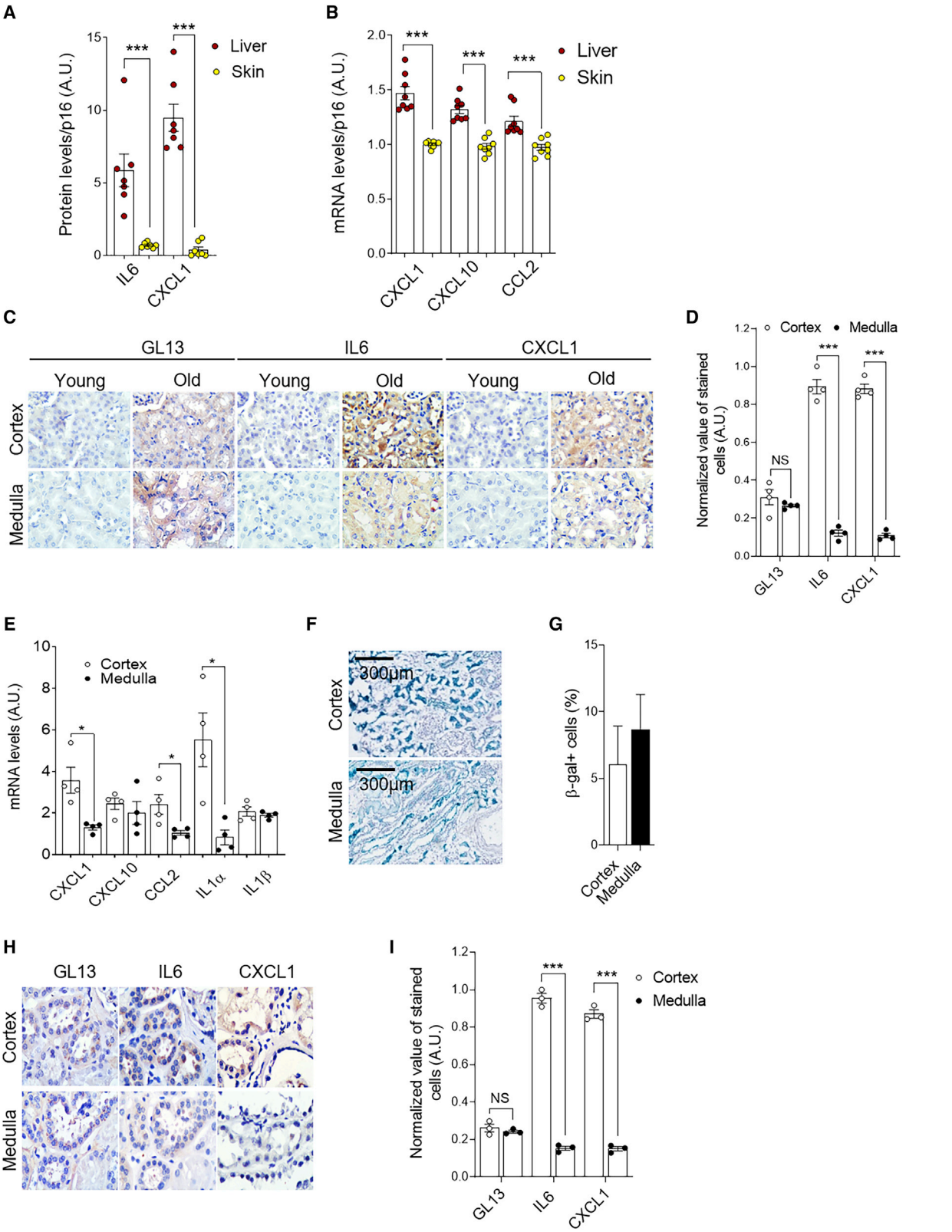

(legend on next page)

pressure. Initially, we focused on naturally aged mice, which have been shown by us and others to accumulate senescent cells in virtually every organ (Demaria et al., 2014; Baker et al., 2016; Yousefzadeh et al., 2020). In the epidermal layers of the skin, oxygen levels are approximately 1% (8 mm Hg) (Wang, et al., 2003), while in the liver pO_2 can reach up to 7% (55 mm Hg) (Leary et al., 2002). mRNA and protein levels of p16 were similarly increased in skin and liver of old mice compared with young (3–6 months) animals, confirming that physiological oxygen has minimal effects on regulation of senescence- and cell-cycle arrest-associated genes (Figures S2A–S2C). However, protein and mRNA levels of various SASP factors were significantly higher in the liver of old animals (Figures 2A and 2B). The kidney has an intra-tissue physiological gradient of oxygen pressure that goes from 10 mm Hg (~1.5%) in the medullary region to up to 70 mm Hg (9%) in the cortical area (Welch, 2006; Rosen et al., 1992; Keeley and Mann, 2019). Immunostaining analysis revealed an equal induction of senescent cells, as measured by the number of lipofuscin-containing (GL13) cells, in the different renal regions of aged mice (Figures 2C and 2D). However, expression of the SASP markers IL-6 and CXCL1 in the medullary region was significantly lower than in the cortex (Figures 2C and 2D). Medullary and cortical areas dissociated from kidneys of old mice show expression of the correct region-specific transcripts (SLGT2 and podocin in the cortex and AQP2 and UPK3a in the medulla; Figure S2D) (Clark et al., 2019) and similar p16 levels (Figure S2E), while the mRNA levels of genes encoding for the SASP factors CXCL1, CCL2, and IL-1α followed the intra-renal oxygen gradient (Figure 2E). Finally, we analyzed expression of senescence and SASP markers in kidney biopsies obtained from human donors. Distribution of SA-βgal$^+$, p16$^+$, or GL13$^+$ cells was similar between the regions (Figures 2F–2I; Figures S2F and S2G), but IL-6 and CXCL1 expression was significantly lower in medullary compared with cortical regions (Figures 2H and 2I). Together, these data show that physiologic hypoxia in tissues is associated with reduced expression of pro-inflammatory SASP factors in both mice and humans.

SASP inhibition is controlled by AMPK-mediated mTOR restriction

In DNA damage-induced senescence, the transcription factor NF-κB is engaged during the DDR and regulates the transcription of pro-inflammatory SASP factors (Kang et al., 2015). When we measured the transcriptional activity of NF-κB in BJ cells exposed to doxo or vehicle, we observed a robust induction in cells treated with TNF-α, used as positive control, or doxo in normoxia, but no significant induction in hypoxia (Figure 3A). Hypoxia inducible factor (HIF)-1α is a major sensor of low-oxygen conditions and can regulate NF-κB activity and the transcription of various pro-inflammatory factors part of the SASP (Scortegagna et al., 2008; Walmsley et al., 2005; Tafani et al., 2011; Vink et al., 2007; Stojanović et al., 2020; Alique et al., 2020). However, transduction of WI-38 cells with lentiviral particles carrying short hairpin against HIF-1α (shHif-1α) (Figures S3A–S3C) did not interfere with senescence induction, as measured by SA-βgal staining (Figure S3D), and was not sufficient to rescue SASP expression in hypoxic senescent cells (Figure S3E). Interestingly, we observed reductions of CXCL1, CXCL10, and CCL2 mRNAs in 5% O_2 senescent cells carrying the shHIF-1α particles (Figure S3E). mTOR is a central regulator of protein synthesis whose activity is modulated by nutrient availability and inhibited by conditions of energy depletion, such as during hypoxia (Brugarolas et al., 2004). In accordance, when we measured levels of phosphorylated ribosomal protein S6 as a surrogate for mTOR activity in kidney sections collected from 24-month-old mice, we observed a robust induction in the cortex region, a tissue area associated with high oxygen and SASP, while the signal was almost absent in the hypoxic and SASP-less medullary region (Figures 3B and 3C). We then analyzed the level of phosphorylated S6 and S6 kinase in doxo-treated BJ cells cultured at 5% or 1% O_2. Western blot analysis revealed enhanced phosphorylation of S6 kinase and S6, downstream effectors of mTOR signaling, in doxo-induced senescent cells cultured at 5% O_2 but not in cells cultured at low oxygen (Figure 3D). Previous studies have shown that the mTOR pathway controls translational regulation of IL-1α to support SASP production (Laberge et al., 2015; Herranz et al., 2015). In accordance with downregulated mTOR activity, hypoxic senescent cells showed a significantly reduced IL-1α expression on the cell membrane (Figure S3F). To evaluate whether forcing mTOR activity could re-enable SASP production in hypoxic conditions, we treated senescent cells cultured at 1% O_2 with the pharmacological mTOR activator MHY1485 or with short hairpins against TSC1, a major inhibitory protein of the mTOR complex whose downregulation causes mTOR hyperactivation (Figures S3G and S3H). Forcing mTOR activity was sufficient to restore NF-κB transcriptional activity and rescued expression of mRNA levels of various SASP factors (Figures 3E–3G).

Figure 2. SASP expression varies among tissues with different oxygen levels

(A) Total protein lysates from skin and liver of old (>24 months) mice were analyzed for IL-6 and CXCL1 levels using ELISA and normalized on protein p16 levels (Figures S2A and S2B). n = 7.

(B) qRT-PCR analysis of RNA isolated from skin and liver of old mice (>24 months). RNA was analyzed for abundance of indicated mRNA levels relative to housekeeping mRNA levels (tubulin) and normalized to p16 mRNA levels. n = 8.

(C and D) Immunohistochemistry staining of kidney tissue sections from old (24 months) or young mice using antibodies against GL13, IL-6, and CXCL1. (C) Representative images and (D) quantification; n = 4.

(E) Total RNA was isolated from cortex and medulla of old mice, and mRNA levels of the indicated genes were quantified using qRT-PCR relative to housekeeping mRNA levels (tubulin) and normalized to p16 mRNA levels. n = 4.

(F and G) Frozen human kidney sections were fixed and stained for SA-βgal. (F) Representative images and (G) quantification; n = 2.

(H and I) Immunohistochemistry was performed on human kidney tissue sections using antibodies against GL13, IL-6, and CXCL1. (H) Representative images and (I) quantification; n = 4.

In (A), (B), (D), (E), and (I), two-tailed t test, *$p < 0.05$, **$p < 0.01$, and ***$p < 0.001$; NS, not significant. A.U., arbitrary units. Data are shown as mean ± SEM. See also Figure S2.

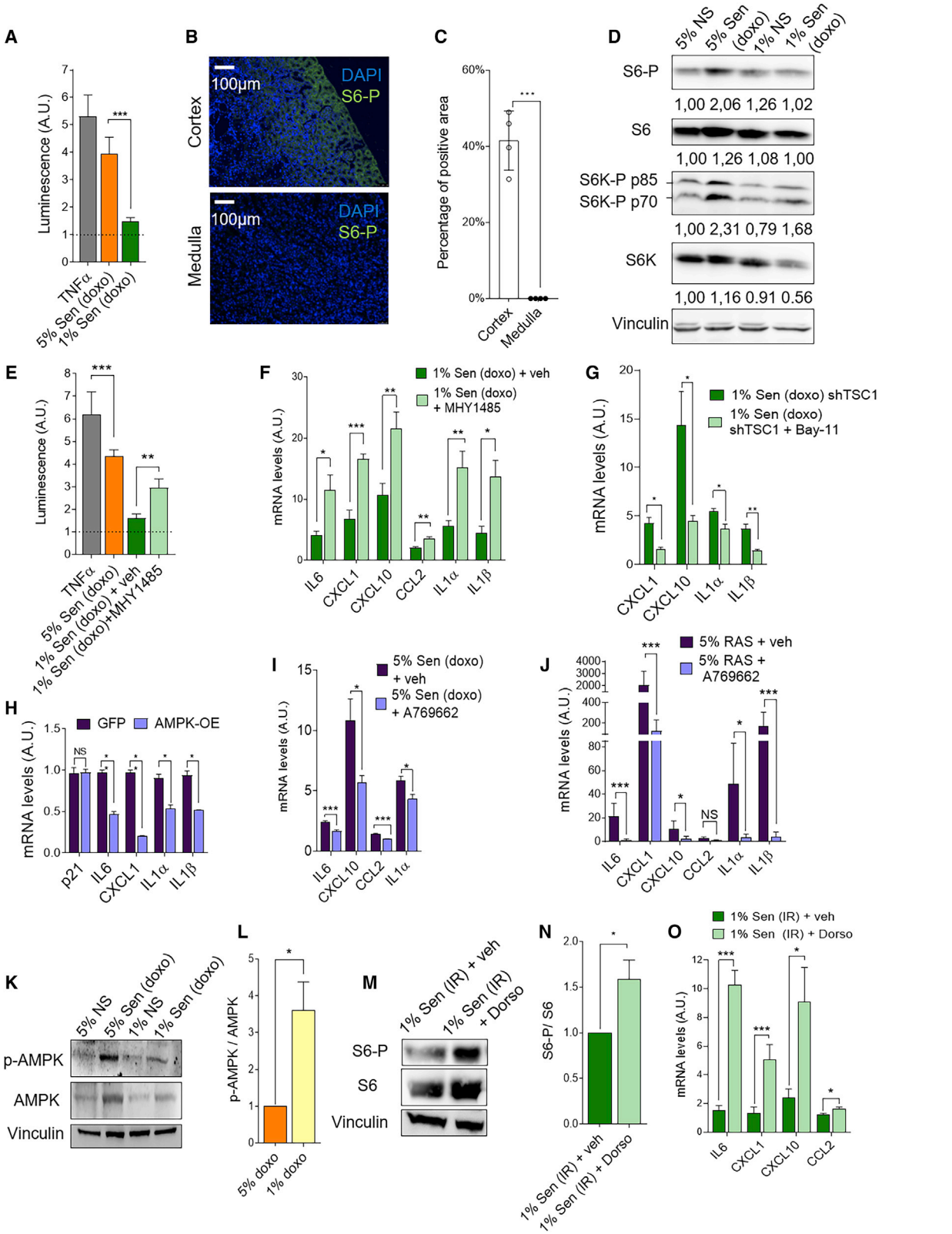

(legend on next page)

Importantly, we also observed that the mTOR-mediated rescue in SASP expression was reversed by the pharmacological NF-κB inhibitor Bay-11 (Figure 3G). Together, these data suggest that during hypoxia, senescent cells fail to activate mTOR signaling, with consequent reduction of NF-κB activity and SASP production.

Multiple mechanisms can inhibit the mTOR pathway, including the AMPK, an intracellular fuel sensor that helps maintain energy balance in low-oxygen environments (González et al., 2020; Yuan et al., 2013). A previous report has shown that metformin, an anti-diabetic drug with multiple molecular functions including activation of AMPK, can reduce the SASP of normoxic senescent cells (Moiseeva et al., 2013). When we forced AMPK activity in normoxic senescent cells via genetic overexpression or treatment with the selective AMPK activator A769662 (Figures S3H–S3J) we observed a reduction of mRNA levels of various SASP factors in senescent BJ and IMR-90 cells (Figures 3H–3J). Importantly, forced AMPK activity was associated with inhibition of mTOR signaling, as shown by almost complete abrogation of S6 phosphorylation (Figure S3K). As senescent cells expressed higher levels of phosphorylated AMPK when cultured in hypoxic conditions (Figures 3K and 3L), we tested if hypoxia-mediated AMPK activity was responsible for preventing mTOR signaling and SASP induction. Strikingly, suppression of AMPK activity, achieved by exposing cells to the pharmacological agent dorsomorphin (Figure S3L), was sufficient to restore mTOR signaling (Figures 3M and 3N) and to rescue the expression of various SASP factors (Figure 3O). Together, these data show that the expression and secretion of pro-inflammatory SASP factors is restrained under physiological hypoxia via an AMPK-mediated suppression of mTOR signaling.

Hypoxia-mimetic compounds reduce an existing SASP in primary cultures and *in vivo*

As exposure of senescent cells to hypoxic conditions was sufficient to prevent SASP induction, we decided to test if hypoxia-mimetic compounds such as roxadustat and 2,3-dihydroxy benzoic acid (DHB) (Selvaraju et al., 2014; Davis et al., 2019) could exert a similar senostatic effect. Treatment with hypoxia mimetics increased the expression roxadustat of hypoxia markers such as MIF-1 and the glycolytic markers GLUT1 and PDK1 (Figure S4A) but did not interfere with senescence induction because of RAS overexpression or doxo treatment in both IMR-90 and BJ cells, as shown by the number of EdU^+ and SA-βgal^+ cells (Figures S4B–S4F). However, treatment with hypoxia mimetics was sufficient to reduce mRNA levels of various SASP factors (Figures 4A and 4B), and this reduction was associated with decreased mTOR signaling and NF-κB activity (Figures 4C and 4D; Figure S4G). In accordance with reduced SASP, CM collected from senescent cells exposed to hypoxia mimetics promoted only marginal pro-migratory effects of MDA-231 cells (Figure 4E; Figures S4H and S4I). To evaluate if hypoxia mimetics could achieve SASP inhibition *in vivo*, we made use of two different mouse models of senescence. For

Figure 3. Hypoxia restrains the SASP via AMPK-mediated mTOR and NF-κB inhibition

(A) BJ cells transduced with a NF-κB reporter were treated with doxo (250 nM, 24 h). Fourteen days after doxo removal, luciferase activity was measured. Dotted line indicates luciferase activity from proliferating cells in normoxia (arbitrary value). TNF-α treatment was used as positive control. n = 9 from three independent experiments.

(B and C) Immunofluorescent staining was performed on kidney tissue sections from old (24 months) mice using an antibody against phosphorylated ribosomal protein S6 (S6-P) and counterstained with DAPI. (B) Representative images and (C) quantification; n = 4.

(D) Western blot analysis of doxo-treated and proliferating BJ cells cultured in 5% or 1% O_2 for 14 days. Numbers represent protein levels relative to vinculin (loading control).

(E) Luciferase activity in doxo-treated BJ cells transduced with a NF-κB reporter and cultured in 1% or 5% O_2 for 14 days or cultured in hypoxia and treated with 10 μM of MHY1485 for 6 h at day 14 after doxo removal. Dotted line indicates luciferase activity from proliferating cells in normoxia (arbitrary value). n = 9 from three independent experiments.

(F) Fourteen days after doxo removal, BJ cells were treated with vehicle (DMSO) or 10 μM of MHY1485 for 6 h. Total RNA was isolated and mRNA levels of the indicated genes quantified using qRT-PCR relative to housekeeping mRNA levels (mean actin/tubulin). n = 6 from two independent experiments.

(G) BJ cells were transduced with lentiviral particles carrying a short hairpin against TSC1 (shTSC1). shTSC1-transduced BJ cells were treated with 1 μM of Bay-11 for 24 h on day 14. Total RNA was analyzed for indicated mRNA levels using qRT-PCR relative to housekeeping mRNA levels (mean actin/tubulin). n = 3 independent experiments.

(H) BJ cells were transduced with virus containing a vector overexpressing either GFP or AMPK upon exposure to doxycycline. Total RNA was isolated, and mRNA levels of the indicated genes were quantified using qRT-PCR relative to housekeeping mRNA levels (tubulin). n = 2.

(I) Doxo-treated BJ cells were cultured for 14 days in 5% O_2 in the presence of vehicle (veh; DMSO) or A769662 (20 μM). Total RNA was isolated, and mRNA levels of the indicated genes were quantified using qRT-PCR relative to housekeeping mRNA levels (mean actin/tubulin). n = 6 from two independent experiments.

(J) IMR-90 cells overexpressing RAS were cultured for 14 days in 5% O_2 in the presence of vehicle (veh; DMSO) or A769662 (20 μM). Total RNA was isolated, and mRNA levels of the indicated genes were quantified using qRT-PCR relative to housekeeping mRNA levels (mean actin/tubulin). n = 9 from three independent experiments.

(K and L) Western blot analysis of BJ cells treated with doxorubicin (250 nM, 24 h) and non-senescent control cells (NS) cultured in 1% or 5% oxygen using antibodies against phosphorylated and total AMPK (p-AMPK and AMPK). Vinculin was used as a loading control. (K) Representative blot and (L) quantification. n = 3 independent experiments.

(M and N) Western blot analysis of IR-treated WI-38 cells cultured for 10 days at 1% O_2 in the presence of vehicle (veh; DMSO) or dorsomorphin (2.5 μM) using antibodies against phosphorylated ribosomal protein S6 and total S6 (S6 and S6-P). Vinculin was used as a loading control. (M) Representative blot and (N) quantification. n = 3 independent experiments.

(O) IR-treated WI-38 cells were cultured for 10 days at 1% O_2 in the presence of vehicle (veh; DMSO) or dorsomorphin (1 μM). Total RNA was isolated, and mRNA levels of the indicated genes were quantified using qRT-PCR relative to housekeeping mRNA levels (mean actin/tubulin). n = 6 from two independent experiments.

In (A), (C), (E)–(J), (L), (N), and (O), two-tailed t test, *$p < 0.05$, **$p < 0.01$, and ***$p < 0.001$; NS, not significant. A.U., arbitrary units. Data are shown as mean ± SEM. See also Figure S3.

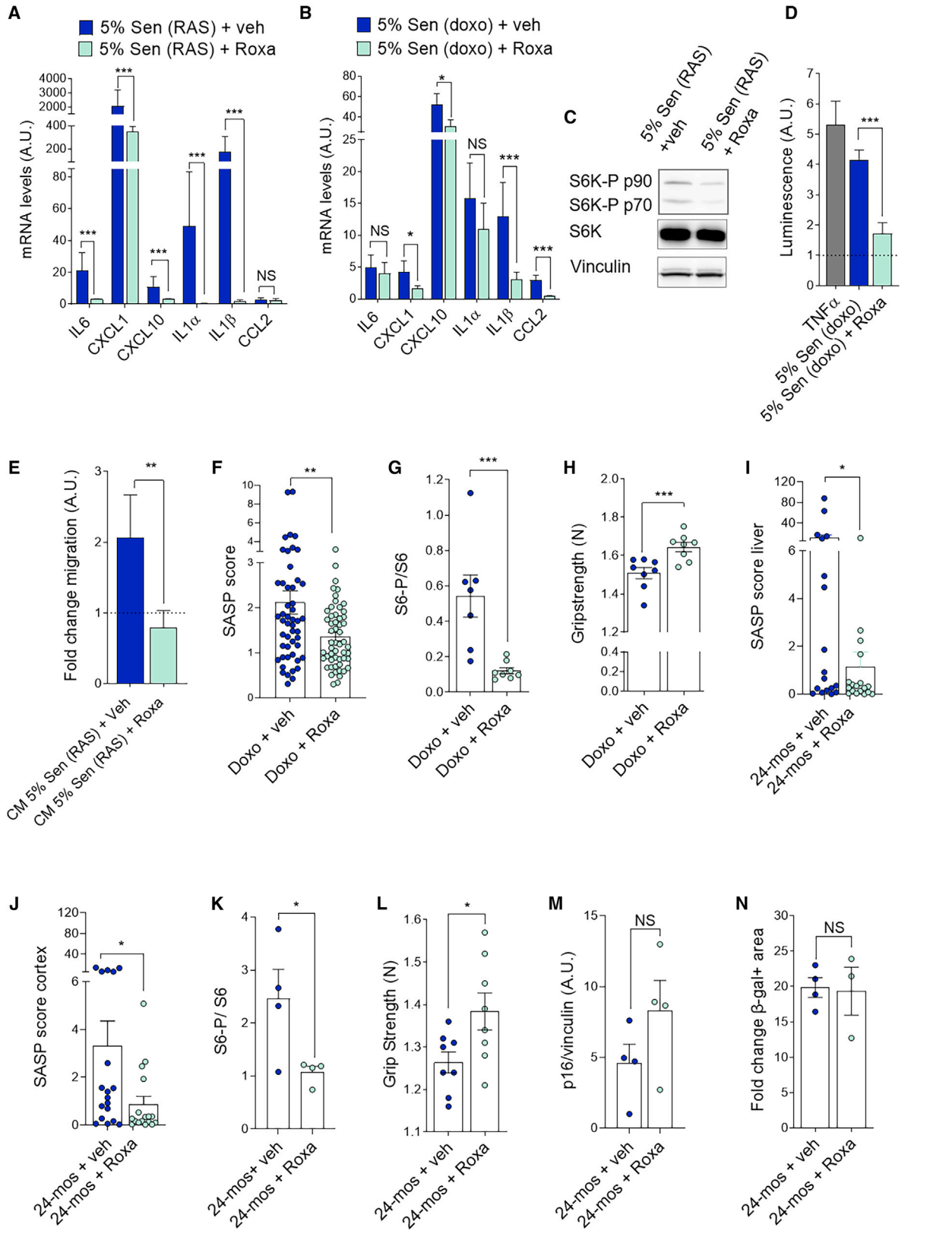

(legend on next page)

the first model, we used mice in which senescence was prematurely induced by doxo. Seven days after doxo treatment, we injected animals with roxadustat for 14 consecutive days. Levels of p21 and p16 expression were upregulated by doxo treatment and not decreased by roxadustat treatment (Figures S4J and S4K). In contrast, roxadustat treatment was sufficient to reduce significantly SASP expression and mTOR activity (Figures 4F and 4G). Roxadustat treatment also significantly attenuated a major chemotherapy-induced side effect, muscle weakness, which we have previously shown to be dependent on the presence of senescent cells with high SASP (Demaria et al., 2017) (Figure 4H).

For the second model, we used aged mice (approximately 24 months) in which senescent cells naturally accumulate. Treatment with roxadustat or DHB significantly decreased the SASP in liver and renal cortical region (Figures 4I and 4J; Figures S4L and S4M), reduced mTOR signaling (Figure 4K) and improved muscle strength (Figure 4L).

Similar to what observed in the doxo model, SASP reduction was not due to senescent cell elimination, as the level of p16 and SA-βgal staining in tissues of mice treated with hypoxia mimetics remained similar to that in control animals (Figures 4M and 4N; Figure S4M). Together, these data show that hypoxia-mimetic compounds can suppress SASP expression and reduce detrimental functions of senescent cells.

DISCUSSION

The expression and secretion of pro-inflammatory SASP factors represent a double-edged sword for the biological function of cellular senescence: on one side, it acts as an immune surveillance mechanism favoring senescent cell removal and potentiating tissue regeneration and remodeling; on the other, it generates chronic inflamed environments and supports tissue dysfunctions (Hernandez-Segura et al., 2018a; Gorgoulis et al., 2019). A novel concept surrounding the paradoxical opposite effect of senescent cells *in vivo* is the existence of distinct subtypes of senescent cells that develop distinguished phenotypes on the basis of epi-genetic and environmental factors (Hernandez-Segura et al., 2018a; Gorgoulis et al., 2019). A major environmental variable in tissues is oxygen availability (Carreau et al., 2011). Here, we have studied how senescence-associated phenotypes develop in different oxygen conditions and demonstrated how oxygen tensions can regulate the development of a pro-inflammatory SASP. It was previously shown that the mTOR-NF-κB axis is an important regulator for the transcription of pro-inflammatory SASP factors (Laberge et al., 2015; Herranz et al., 2015) and that hypoxia impairs mTOR function (Brugarolas et al., 2004). In accordance, we demonstrate that senescent cells under hypoxia fail to mount a robust activation of mTOR, with consequent reduction of NF-κB and SASP inductions. Moreover, we show that this reduced mTOR activity in hypoxic senescent cells is mediated by a major fuel sensor and hypoxia regulator, AMPK. This mechanism might be at the basis of the anti-SASP effects observed in other conditions that activate AMPK (Palacios et al., 2009; Edwards et al., 2010). For example, both caloric restriction and exercise have been shown to decrease senescence markers (Schafer et al., 2016; Fontana et al., 2018), and caloric restriction has been shown to inhibit inflammation and NF-κB activity (Matsuzaki et al., 2001; Jung et al., 2009). Our data provide a possible link between these conditions and their anti-inflammatory effects that can be further explored. We also show that SASP repression under hypoxia is independent from HIF-1α but that abrogation of HIF-1α under normoxia restrains SASP expression. Considering the hypoxia-independent pro-inflammatory activity of HIF-1α (Jung et al., 2003; Scortegagna et al., 2008; Walmsley et al., 2005; Tafani et al., 2011) and previous suggestions of an important role of HIF-1 in regulating

Figure 4. Hypoxia-mimetic compounds reduce SASP levels in culture and *in vivo*

(A–C) RAS-overexpressing IMR-90 cells were cultured for 10 days in 5% O_2 and treated with vehicle (veh; DMSO),or roxadustat (50 μM). (A and B) Total RNA was isolated, and mRNA levels of the indicated genes were quantified using qRT-PCR relative to housekeeping mRNA levels (mean actin/tubulin). (A) n = 12 from four independent experiments. (B) n = 9 from three independent experiments. (C) Western blot analysis using antibodies against phosphorylated and total ribosomal protein S6 kinase (S6K and S6K-P). p90 and p70 represent the different subunits of S6K. Vinculin was used as a loading control.

(D) BJ cells transduced with a NF-κB reporter were treated with doxo (250 nM, 24 h) and cultured in 5% O_2 in the presence of vehicle (DMSO) or roxadustat (50 μM). Fourteen days after doxo removal, luciferase activity was measured. Dotted line indicates luciferase activity from proliferating cells 5% O_2 (arbitrary value set at 1). TNF-α treatment was used as positive control. n = 9 from three independent experiments.

(E) Migration of MDA-231 cells exposed to CM collected from RAS-IMR-90 cells treated with vehicle (DMSO) or roxadustat (50 μM) was measured using transwells. Dotted line represents migration of MDA-231 cells exposed to CM from ctrl cells set at 1 for each experiment. n = 9 from three independent experiments.

(F–H) Mice were treated with 5 mg/kg of doxorubicin for 3 consecutive days. One week later, mice were injected with roxadustat (10 mg/kg, 14 consecutive days), and livers were harvested for analysis. n = 8. (F) Total RNA was isolated, mRNA levels of the indicated genes were quantified using qRT-PCR relative to housekeeping mRNA levels (mean actin/tubulin), and a SASP score was calculated pooling the ΔΔCq gene's values of IL-6, IL-1β, IL-1α, CXCL1, CXCL10, CCL2, CCL20, and GDNF10. (G) Protein lysates of liver were analyzed for phosphorylated and total ribosomal protein S6 (S6-P and S6) levels using western blot. (H) Grip strength of forelimbs was measured using a grip-strength meter 1 day after the last roxadustat treatment.

(I–N) Old P16-3MR mice (~24 months) were treated with 30 mg/kg of roxadustat three times once every 2 days. From a subset of the mice, RFP^+ cells were sorted from the renal cortex and liver using fluorescence-activated cell sorting (FACS). From another subset of animals, total liver and renal cortex were collected for further analysis. (I and J) RFP^+ cells were collected from liver (I) and cortex (J), total RNA was isolated, mRNA levels of the indicated genes quantified using qRT-PCR relative to housekeeping mRNA levels (tubulin), and a SASP score was calculated pooling the ΔΔCq gene's values of IL-6, IL-1β, IL-1α, CXCL1, CXCL10, and CCL2. n = 18. (K) Western blot analysis using protein lysates from cortex using antibodies against phosphorylated ribosomal protein S6 and total S6 (S6-P and S6). Vinculin was used as a loading control. n = 4. (L) Grip strength of forelimbs was measured using a grip-strength meter. (M) Western blot analysis using protein lysates from liver using and antibody against p16. Vinculin was used as a loading control. n = 4. (N) Quantification of SA-βgal staining performed on frozen section of the cortex. n = 4.

In (A), (B), and (D)–(N), two-tailed t test, $^*p < 0.05$, $^{**}p < 0.01$, and $^{***}p < 0.001$; NS, not significant. A.U., arbitrary units. Data are shown as mean ± SEM. See also Figure S4.

senescence-associated properties (Welford et al., 2006; Zhu et al., 2015), our data prime research aiming at exploring the role of HIF-1α in SASP regulation and testing the effects of drugs that modulate HIF-1α on senescent cells. Finally, we have shown that intermittent treatment with hypoxia mimetics, a class of compounds that mimic the effects of hypoxic conditions, can reduce SASP expression in mice with prematurely or naturally high levels of senescence without interfering with senescent cells survival. Importantly, these treatments resulted in alleviation of muscle weakness and strength, a major detrimental effect caused by persistent senescence and chronic SASP (Demaria et al., 2017). Our data open up new possibilities for the development of interventions including treatment with hypoxia mimetics or intermittent exposure to hypoxic conditions to battle the deleterious effects of senescent cells.

STAR★METHODS

Detailed methods are provided in the online version of this paper and include the following:

- KEY RESOURCES TABLE
- RESOURCE AVAILABILITY
  - Lead contact
  - Materials availability
  - Data and code availability
- EXPERIMENTAL MODEL AND SUBJECT DETAILS
  - Cell culture and treatments
  - Mice
- METHOD DETAILS
  - Cell morphology analysis
  - EdU staining
  - Senescence-associated β-galactosidase staining
  - Immunofluorescence
  - Real-time PCR
  - Protein sample preparation and enzyme-linked immunosorbent assays (ELISA)
  - Transwell migration assay
  - Immunohistochemistry
  - Immunoblot analysis
  - Detection of cell surface-bound IL1α using FACS
  - Generation of lentiviral NF-kB reporter vector
  - Generation of lentiviral particles
  - Lentivirus transduction
- QUANTIFICATION AND STATISTICAL ANALYSIS

SUPPLEMENTAL INFORMATION

Supplemental information can be found online at https://doi.org/10.1016/j.molcel.2021.03.018.

ACKNOWLEDGMENTS

We thank Alain de Bruin and Mirjam Koster for help with staining of kidney sections. We are thankful to the Demaria laboratory for fruitful discussions. M.D. is funded by grants from the Dutch Cancer Foundation (KWF). K.E. and V.G. were financially supported by the European Union's Horizon 2020 research and innovation program under Marie Skłodowska-Curie grant agreement 722729 (SYNTRAIN); the National Public Investment Program of the Ministry of Development and Investment/General Secretariat for Research and Technology, in the framework of the Flagship Initiative to address SARS-CoV-2 (2020ΣΕ01300001); the Welfare Foundation for Social & Cultural Sciences (KIKPE), Greece; a donation from H. Pappas; grant 775 from the Hellenic Foundation for Research and Innovation (HFRI); and National and Kapodistrian University of Athens (NKUA) Special Account for Research Grants (SARG) grants 70/3/9816, 70/3/12128, and 70/3/15603.

AUTHOR CONTRIBUTIONS

Conceptualization, T.V. and M.D.; Data Curation, T.V., R.F., V.G., and M.D.; Formal Analysis, T.V., M.V.-E., B.W., M.B., K.E., R.F., V.G., and M.D.; Funding Acquisition, M.S., V.G., and M.D.; Investigation, T.V., M.V.-E., B.W., M.B., S.M.B., K.E., R.F., V.G., and M.D.; Methodology, T.V., M.V.-E., B.W., M.B., S.M.B., K.E., R.F., V.G., and M.D.; Project Administration, M.D.; Resources, V.G. and M.D.; Supervision, M.D.; Validation, T.V., M.V.-E., B.W., M.B., S.M.B., K.E., R.F., V.G., and M.D.; Visualization, T.V. and M.D.; Writing – Original Draft, T.V. and M.D.; Writing – Review & Editing, T.V., M.V.-E., B.W., M.B., S.M.B., K.E., R.F., V.G., and M.D.

DECLARATION OF INTERESTS

M.D. is scientific co-founder, advisor, and shareholder of Cleara Biotech. However, the manuscript was not influenced or funded by Cleara Biotech.

INCLUSION AND DIVERSITY

We worked to ensure sex balance in the selection of non-human subjects and cell lines.

Received: June 30, 2020
Revised: January 21, 2021
Accepted: March 11, 2021
Published: April 5, 2021

REFERENCES

Alique, M., Sánchez-López, E., Bodega, G., Giannarelli, C., Carracedo, J., and Ramírez, R. (2020). Hypoxia-inducible factor-1α: the master regulator of endothelial cell senescence in vascular aging. Cells *9*, 195.

Ast, T., and Mootha, V.K. (2019). Oxygen and mammalian cell culture: are we repeating the experiment of Dr. Ox? Nat. Metab. *1*, 858–860.

Baker, D.J., Childs, B.G., Durik, M., Wijers, M.E., Sieben, C.J., Zhong, J., Saltness, R.A., Jeganathan, K.B., Verzosa, G.C., Pezeshki, A., et al. (2016). Naturally occurring p16(Ink4a)-positive cells shorten healthy lifespan. Nature *530*, 184–189.

Blagosklonny, M.V. (2014). Geroconversion: irreversible step to cellular senescence. Cell Cycle *13*, 3628–3635.

Brugarolas, J., Lei, K., Hurley, R.L., Manning, B.D., Reiling, J.H., Hafen, E., Witters, L.A., Ellisen, L.W., and Kaelin, W.G., Jr. (2004). Regulation of mTOR function in response to hypoxia by REDD1 and the TSC1/TSC2 tumor suppressor complex. Genes Dev. *18*, 2893–2904.

Carreau, A., El Hafny-Rahbi, B., Matejuk, A., Grillon, C., and Kieda, C. (2011). Why is the partial oxygen pressure of human tissues a crucial parameter? Small molecules and hypoxia. J. Cell. Mol. Med. *15*, 1239–1253.

Casciaro, F., Borghesan, M., Beretti, F., Zavatti, M., Bertucci, E., Follo, M.Y., Maraldi, T., and Demaria, M. (2020). Prolonged hypoxia delays aging and preserves functionality of human amniotic fluid stem cells. Mech. Ageing Dev. *191*, 111328.

Chen, Q., Fischer, A., Reagan, J.D., Yan, L.J.A.D.J., and Ames, B.N. (1995). Oxidative DNA damage and senescence of human diploid fibroblast cells. Proc. Natl. Acad. Sci. U S A *92*, 4337–4341.

Clark, J.Z., Chen, L., Chou, C.L., Jung, H.J., Lee, J.W., and Knepper, M.A. (2019). Representation and relative abundance of cell-type selective markers in whole-kidney RNA-seq data. Kidney Int. *95*, 787–796.

Coppé, J.P., Patil, C.K., Rodier, F., Krtolica, A., Beauséjour, C.M., Parrinello, S., Hodgson, J.G., Chin, K., Desprez, P.Y., and Campisi, J. (2010). A human-

like senescence-associated secretory phenotype is conserved in mouse cells dependent on physiological oxygen. PLoS ONE *5*, e9188.

Davis, C.K., Jain, S.A., Bae, O.-N., Majid, A., and Rajanikant, G.K. (2019). Hypoxia mimetic agents for ischemic stroke. Front. Cell Dev. Biol. *6*, 175.

Demaria, M., Ohtani, N., Youssef, S.A., Rodier, F., Toussaint, W., Mitchell, J.R., Laberge, R.M., Vijg, J., Van Steeg, H., Dollé, M.E.T., et al. (2014). An essential role for senescent cells in optimal wound healing through secretion of PDGF-AA. Dev. Cell *31*, 722–733.

Demaria, M., O'Leary, M.N., Chang, J., Shao, L., Liu, S., Alimirah, F., Koenig, K., Le, C., Mitin, N., Deal, A.M., et al. (2017). Cellular senescence promotes adverse effects of chemotherapy and cancer relapse. Cancer Discov. *7*, 165–176.

Edwards, A.G., Donato, A.J., Lesniewski, L.A., Gioscia, R.A., Seals, D.R., and Moore, R.L. (2010). Life-long caloric restriction elicits pronounced protection of the aged myocardium: a role for AMPK. Mech. Ageing Dev. *131*, 739–742.

Fontana, L., Mitchell, S.E., Wang, B., Tosti, V., van Vliet, T., Veronese, N., Bertozzi, B., Early, D.S., Maissan, P., Speakman, J.R., and Demaria, M. (2018). The effects of graded caloric restriction: XII. Comparison of mouse to human impact on cellular senescence in the colon. Aging Cell *17*, e12746.

González, A., Hall, M.N., Lin, S.C., and Hardie, D.G. (2020). AMPK and TOR: the yin and yang of cellular nutrient sensing and growth control. Cell Metab. *31*, 472–492.

Gorgoulis, V., Adams, P.D., Alimonti, A., Bennett, D.C., Bischof, O., Bishop, C., Campisi, J., Collado, M., Evangelou, K., Ferbeyre, G., et al. (2019). Cellular senescence: defining a path forward. Cell *179*, 813–827.

Hernandez-Segura, A., Brandenburg, S., and Demaria, M. (2018a). Induction and validation of cellular senescence in primary human cells. J. Vis. Exp. *136*, e57782.

Hernandez-Segura, A., Nehme, J., and Demaria, M. (2018b). Hallmarks of cellular senescence. Trends Cell Biol. *28*, 436–453.

Herranz, N., Gallage, S., Mellone, M., Wuestefeld, T., Klotz, S., Hanley, C.J., Raguz, S., Acosta, J.C., Innes, A.J., Banito, A., et al. (2015). mTOR regulates MAPKAPK2 translation to control the senescence-associated secretory phenotype. Nat. Cell Biol. *17*, 1205–1217.

Jung, Y., Isaacs, J.S., Lee, S., Trepel, J., Liu, Z.G., and Neckers, L. (2003). Hypoxia-inducible factor induction by tumour necrosis factor in normoxic cells requires receptor-interacting protein-dependent nuclear factor kappa B activation. Biochem. J. *370*, 1011–1017.

Jung, K.J., Lee, E.K., Kim, J.Y., Zou, Y., Sung, B., Heo, H.S., Kim, M.K., Lee, J., Kim, N.D., Yu, B.P., and Chung, H.Y. (2009). Effect of short term calorie restriction on pro-inflammatory NF-kB and AP-1 in aged rat kidney. Inflamm. Res. *58*, 143–150.

Kang, C., Xu, Q., Martin, T.D., Li, M.Z., Demaria, M., Aron, L., Lu, T., Yankner, B.A., Campisi, J., and Elledge, S.J. (2015). The DNA damage response induces inflammation and senescence by inhibiting autophagy of GATA4. Science *349*, aaa5612.

Keeley, T.P., and Mann, G.E. (2019). Defining physiological normoxia for improved translation of cell physiology to animal models and humans. Physiol. Rev. *99*, 161–234.

Kilic Eren, M., and Tabor, V. (2014). The role of hypoxia inducible factor-1 alpha in bypassing oncogene-induced senescence. PLoS ONE *9*, e101064.

Laberge, R.M., Sun, Y., Orjalo, A.V., Patil, C.K., Freund, A., Zhou, L., Curran, S.C., Davalos, A.R., Wilson-Edell, K.A., Liu, S., et al. (2015). MTOR regulates the pro-tumorigenic senescence-associated secretory phenotype by promoting IL1A translation. Nat. Cell Biol. *17*, 1049–1061.

Leary, T.S., Klinck, J.R., Hayman, G., Friend, P., Jamieson, N.V., and Gupta, A.K. (2002). Measurement of liver tissue oxygenation after orthotopic liver transplantation using a multiparameter sensor. A pilot study. Anaesthesia *57*, 1128–1133.

Leontieva, O.V., Natarajan, V., Demidenko, Z.N., Burdelya, L.G., Gudkov, A.V., and Blagosklonny, M.V. (2012). Hypoxia suppresses conversion from proliferative arrest to cellular senescence. Proc. Natl. Acad. Sci. U S A *109*, 13314–13318.

Matsuzaki, J., Kuwamura, M., Yamaji, R., Inui, H., and Nakano, Y. (2001). Inflammatory responses to lipopolysaccharide are suppressed in 40% energy-restricted mice. J. Nutr. *131*, 2139–2144.

Moiseeva, O., Deschênes-Simard, X., St-Germain, E., Igelmann, S., Huot, G., Cadar, A.E., Bourdeau, V., Pollak, M.N., and Ferbeyre, G. (2013). Metformin inhibits the senescence-associated secretory phenotype by interfering with IKK/NF-κB activation. Aging Cell *12*, 489–498.

Muñoz-Espín, D., Cañamero, M., Maraver, A., Gómez-López, G., Contreras, J., Murillo-Cuesta, S., Rodríguez-Baeza, A., Varela-Nieto, I., Ruberte, J., Collado, M., and Serrano, M. (2013). Programmed cell senescence during mammalian embryonic development. Cell *155*, 1104–1118.

Murali, B., Ren, Q., Luo, X., Faget, D.V., Wang, C., Johnson, R.M., Gruosso, T., Flanagan, K.C., Fu, Y., Leahy, K., et al. (2018). Inhibition of the stromal p38MAPK/MK2 pathway limits breast cancer metastases and chemotherapy-induced bone loss. Cancer Res. *78*, 5618–5630.

Ortiz-Prado, E., Dunn, J.F., Vasconez, J., Castillo, D., and Viscor, G. (2019). Partial pressure of oxygen in the human body: a general review. Am. J. Blood Res. *9*, 1–14.

Palacios, O.M., Carmona, J.J., Michan, S., Chen, K.Y., Manabe, Y., Ward, J.L., 3rd, Goodyear, L.J., and Tong, Q. (2009). Diet and exercise signals regulate SIRT3 and activate AMPK and PGC-1alpha in skeletal muscle. Aging (Albany NY) *1*, 771–783.

Parrinello, S., Samper, E., Krtolica, A., Goldstein, J., Melov, S., and Campisi, J. (2003). Oxygen sensitivity severely limits the replicative lifespan of murine fibroblasts. Nat. Cell Biol. *5*, 741–747.

Ritschka, B., Storer, M., Mas, A., Heinzmann, F., Ortells, M.C., Morton, J.P., Sansom, O.J., Zender, L., and Keyes, W.M. (2017). The senescence-associated secretory phenotype induces cellular plasticity and tissue regeneration. Genes Dev. *31*, 172–183.

Rosen, S., Epstein, F.H., and Brezis, M. (1992). Determinants of intrarenal oxygenation: factors in acute renal failure. Ren. Fail. *14*, 321–325.

Schafer, M.J., White, T.A., Evans, G., Tonne, J.M., Verzosa, G.C., Stout, M.B., Mazula, D.L., Palmer, A.K., Baker, D.J., Jensen, M.D., et al. (2016). Exercise prevents diet-induced cellular senescence in adipose tissue. Diabetes *65*, 1606–1615.

Scortegagna, M., Cataisson, C., Martin, R.J., Hicklin, D.J., Schreiber, R.D., Yuspa, S.H., and Arbeit, J.M. (2008). HIF-1α regulates epithelial inflammation by cell autonomous NFkappaB activation and paracrine stromal remodeling. Blood *111*, 3343–3354.

Selvaraju, V., Parinandi, N.L., Adluri, R.S., Goldman, J.W., Hussain, N., Sanchez, J.A., and Maulik, N. (2014). Molecular mechanisms of action and therapeutic uses of pharmacological inhibitors of HIF-prolyl 4-hydroxylases for treatment of ischemic diseases. Antioxid. Redox Signal. *20*, 2631–2665.

Stojanović, S.D., Fiedler, J., Bauersachs, J., Thum, T., and Sedding, D.G. (2020). Senescence-induced inflammation: an important player and key therapeutic target in atherosclerosis. Eur. Heart J. *41*, 2983–2996.

Storer, M., Mas, A., Robert-Moreno, A., Pecoraro, M., Ortells, M.C., Di Giacomo, V., Yosef, R., Pilpel, N., Krizhanovsky, V., Sharpe, J., and Keyes, W.M. (2013). Senescence is a developmental mechanism that contributes to embryonic growth and patterning. Cell *155*, 1119–1130.

Sun, Y., Campisi, J., Higano, C., Beer, T.M., Porter, P., Coleman, I., True, L., and Nelson, P.S. (2012). Treatment-induced damage to the tumor microenvironment promotes prostate cancer therapy resistance through WNT16B. Nat. Med. *18*, 1359–1368.

Tafani, M., Schito, L., Pellegrini, L., Villanova, L., Marfe, G., Anwar, T., Rosa, R., Indelicato, M., Fini, M., Pucci, B., and Russo, M.A. (2011). Hypoxia-increased RAGE and P2X7R expression regulates tumor cell invasion through phosphorylation of Erk1/2 and Akt and nuclear translocation of NF-κB. Carcinogenesis *32*, 1167–1175.

Vink, A., Schoneveld, A.H., Lamers, D., Houben, A.J.S., van der Groep, P., van Diest, P.J., and Pasterkamp, G. (2007). HIF-1 alpha expression is associated with an atheromatous inflammatory plaque phenotype and upregulated in activated macrophages. Atherosclerosis *195*, e69–e75.

Walmsley, S.R., Print, C., Farahi, N., Peyssonnaux, C., Johnson, R.S., Cramer, T., Sobolewski, A., Condliffe, A.M., Cowburn, A.S., Johnson, N., and Chilvers, E.R. (2005). Hypoxia-induced neutrophil survival is mediated by HIF-1α-dependent NF-kappaB activity. J. Exp. Med. *201*, 105–115.

Wang, W., Winlove, C.P.M.C.C., and Michel, C.C. (2003). Oxygen partial pressure in outer layers of skin of human finger nail folds. J. Physiol. *549*, 855–863.

Welch, W.J. (2006). Intrarenal oxygen and hypertension. Clin. Exp. Pharmacol. Physiol. *33*, 1002–1005.

Welford, S.M., Bedogni, B., Gradin, K., Poellinger, L., Broome Powell, M., and Giaccia, A.J. (2006). HIF1α delays premature senescence through the activation of MIF. Genes Dev. *20*, 3366–3371.

Wenger, R.H. (2002). Cellular adaptation to hypoxia: O_2-sensing protein hydroxylases, hypoxia-inducible transcription factors, and O_2-regulated gene expression. FASEB J. *16*, 1151–1162.

Xu, M., Pirtskhalava, T., Farr, J.N., Weigand, B.M., Palmer, A.K., Weivoda, M.M., Inman, C.L., Ogrodnik, M.B., Hachfeld, C.M., Fraser, D.G., et al. (2018). Senolytics improve physical function and increase lifespan in old age. Nat. Med. *24*, 1246–1256.

Xu, M., Tchkonia, T., Ding, H., Ogrodnik, M., Lubbers, E.R., Pirtskhalava, T., White, T.A., Johnson, K.O., Stout, M.B., Mezera, V., et al. (2015). JAK inhibition alleviates the cellular senescence-associated secretory phenotype and frailty in old age. Proc. Natl. Acad. Sci. U S A *112*, E6301–E6310.

Yousefzadeh, M.J., Zhao, J., Bukata, C., Wade, E.A., McGowan, S.J., Angelini, L.A., Bank, M.P., Gurkar, A.U., McGuckian, C.A., Calubag, M.F., et al. (2020). Tissue specificity of senescent cell accumulation during physiologic and accelerated aging of mice. Aging Cell *19*, e13094.

Yousefzadeh, M.J., Zhu, J., McGowan, S.J., Angelini, L., Fuhrmann-Stroissnigg, H., Xu, M., Ling, Y.Y., Melos, K.I., Pirtskhalava, T., Inman, C.L., et al. (2018). Fisetin is a senotherapeutic that extends health and lifespan. EBioMedicine *36*, 18–28.

Yuan, H.X., Xiong, Y., and Guan, K.L. (2013). Nutrient sensing, metabolism, and cell growth control. Mol. Cell *49*, 379–387.

Zhu, Y., Tchkonia, T., Pirtskhalava, T., Gower, A.C., Ding, H., Giorgadze, N., Palmer, A.K., Ikeno, Y., Hubbard, G.B., Lenburg, M., et al. (2015). The Achilles' heel of senescent cells: from transcriptome to senolytic drugs. Aging Cell *14*, 644–658.

STAR★METHODS

KEY RESOURCES TABLE

REAGENT or RESOURCE	SOURCE	IDENTIFIER
Antibodies		
Rabbit polyclonal anti-ϒ-H2AX	Novus Biologicals	Cat# NB100-384; RRID:AB_10002815
Rabbit monoclonal anti-Phospho-S6 Ribosomal Protein (Ser235/236)	Cell signaling	Cat# 4858; RRID:AB_390782
Rabbit monoclonal anti-S6 Ribosomal Protein	Cell signaling	Cat# 2217; RRID:AB_331355
Rabbit polyclonal anti-Phospho-p70 S6 Kinase (Thr389)	Cell signaling	Cat# 9205; RRID:AB_330944
Rabbit polyclonal anti-p70 S6 Kinase	Cell signaling	Cat# 9202; RRID:AB_331676
Rabbit polyclonal anti-Phospho-AMPKα (Thr172)	Cell signaling	Cat# 2531; RRID:AB_330330
Rabbit polyclonal anti-Phospho-mTOR (Ser2448)	Cell signaling	Cat# 2971; RRID:AB_330970
Mouse monoclonal anti-AMPK1/2α	Santa Cruz Biotechnology	Cat# sc-74461; RRID:AB_1118940
Mouse monoclonal anti-HIF1α	BD Biosciences	Cat# 610958; RRID:AB_398271
Mouse monoclonal anti-Actin	MP Biomedicals	Cat# 06891001
Mouse monoclonal anti-Vinculin	Sigma-Aldrich	Cat# V9131; RRID:AB_477629
Mouse monoclonal anti- IL-1 alpha /IL-1F1 Membrane Form	R&D systems	Cat# FAB200F; RRID:AB_357119
Rabbit polyclonal anti-IL-6	Abcam	Cat# ab6672-200; RRID:AB_2127460
Rabbit polyclonal anti-CXCL1	Thermo Fisher	Cat# PA5-86508; RRID:AB_2803283
GL13 (Sentragor®)	Lab Supplies Scientific	Cat# AR8850020
Mouse monoclonal anti-biotin	Abcam	Cat# ab201341; RRID:AB_2861249
Bacterial and virus strains		
NEB stable Competent *E. coli* (High Efficiency	New England Biolabs (NEB)	Cat# c3040h
Lentiviral particle produced using ViraPower plasmid mix	Invitrogen	Cat# K4970-00
Biological samples		
Human Kidney tissue	Gift from dr. Marc Seelen, University Medical center Groningen	N/A
Chemicals, peptides, and recombinant proteins		
Doxorubicin hydrochloride	Tebu-bio	Cat# BIA-D1202-1
Dorsomorphin	Apex Bio	Cat# B1372
MHY1485	Axon Med Chem	Cat# 2425
A769662	Med Chem Express,	Cat# HY-50662
Bay 11-7082	Med Chem Express	Cat # HY-13453
4-hydroxy-tamoxifen	Sigma-Aldrich	Cat# T176-10MG
Recombinant Human TNF-α	Preprotech	Cat# 300-01A
2,3 dihydroxybenzoic acid	Sigma-Aldrich	Cat# 37580
Roxadustat (FG-4592)	Med Chem Express	Cat# HY-13426
Critical commercial assays		
CycLex® AMPK Kinase Assay Kit	Sanbio	Cat# CY-1182
SensiFast Probe kit	Bioline	Cat# BIO-84020
Luciferase Assay System	Promega	Cat# E1500

(*Continued on next page*)

Continued

REAGENT or RESOURCE	SOURCE	IDENTIFIER
Experimental models: Cell lines		
Proximal tubular epithelial cells (PTEC)	Gift from dr. Marc Seelen, University Medical center Groningen	N/A
Human triple negative breast cancer cells, MDA231	Gift from prof. C.F. Calkhoven, University Medical center Groningen	N/A
Human normal lung fibroblasts, WI38	ATCC	CRL-7728
Human normal foreskin fibroblasts, BJ	ATCC	CRL-2522
Human normal lung fibroblasts, IMR90	ATCC	CRL-7931
Experimental models: Organisms/strains		
Mouse: aged C57BL/6J	Mouse clinic for Cancer and Aging, University Medical Center Groningen (UMCG)	N/A
Mouse: p16-3MR	Demaria et al., 2014	N/A
Oligonucleotides		
Primers for RT-qPCR see Table S1	This manuscript	N/A
Primer for NF-kB response element. Forward: 5′-aaaaatcgatggcctaactggcggtac-3′,	This manuscript	N/A
Primer for NF-kB response element. Reverse: 5′aaaaaggatcccgactctagagtcgcggcc-3′	This manuscript	N/A
shRNAs against Hif-1alpha (MISSION shRNA libray) Sequence: GTGATGAAAGAATTACCGAAT	Sigma Aldrich	TRCN0000003810
Recombinant DNA		
Vector for AMPK overexpression	Addgene	Cat# 74446
Vector for expression of shTSC1	Gift from prof. C.F. Calkhoven, University Medical center Groningen.	N/A
Vector NF-kB-luc, Plasmid pGL4.32 [Luc2P/NF-κB-RE/Hygro]	Promega	Cat# 8491
lentiviral NF-κB-reporter vector (pLenti-NF-κB-RE-minP-LUC-EGFP-hygro)	This manuscript	N/A
Vector for overexpression of mutated RAS	Thermo Fisher Scientific	Cat# 11811031

RESOURCE AVAILABILITY

Lead contact

Further information and requests for resources and reagents should be directed to and will be fulfilled by the Lead Contact: Marco Demaria, m.demaria@umcg.nl

Materials availability

Plasmids generated in this study will be available upon request to the lead contact.

This study did not generate new unique reagents or mouse lines.

Data and code availability

This study did not generate codes or analyze datasets.

EXPERIMENTAL MODEL AND SUBJECT DETAILS

Cell culture and treatments

BJ (CRL-2522), WI38 (CRL-7728), IMR90 (CRL-7931) were obtained from ATCC. MDA231 cells were a gift from prof. Cornelis F. Calkhoven (University Medical Center Groningen, Netherlands). Proximal tubular epithelial cells (PTEC) cells were a gift from dr. Marc Seelen (University Medical Center Groningen). Cells were not re-authenticated by the laboratory but were regularly tested

for mycoplasma contaminations (at least once a month). All cells were cultured in DMEM- glutaMAX pyruvate medium (Thermo Fisher) supplemented with 10% fetal bovine serum (GE healthcare life sciences and Thermo Fisher) and 1% penicillin-streptomycin (Lonza). All cells were cultured in 5% O_2, 5% CO_2, 90% N_2 or 1% O_2, 5% CO_2, 94% N_2, 37°C incubators. Doxorubicin hydrochloride (Tebu-bio, BIA-D1202-1) was dissolved in sterile milliQ water at 250 μM as stock. MHY1485 (Axon Med Chem, Cat# 2425) was dissolved in DMSO at 10mM as stock. A769662 (Med Chem Express, Cat# HY-50662) was dissolved in DMSO at 10mM as stock. Dorsomorphin (Apex Bio, Cat# B1372) was dissolved in DMSO at 10mM stock. 4-hydroxy-tamoxifen (Sigma-Aldrich) was dissolved in ethanol at 10mg/ml as stock. Stock solutions were further diluted in DMEM medium mentioned above as indicated in each figure legend. To induce senescence by ionizing radiation, cells were plated in T75 culture flasks at 60%–70% confluency and treated with 10Gy of γ-radiation from a Cesium 137 source. To induce senescence by oncogenic activation, IMR90 cells were transduced with lentiviral particles encoding for tamoxifen inducible RAS oncogene (RASVal12) and stimulated with 200nM of tamoxifen for 6 consecutive days (3*48 h) Senescence inducing drug treatments were applied to cells cultured in 5% O_2, 5% CO_2, 90% N_2, 37°C incubators and subsequently maintained at oxygen conditions indicated in each figure.

Mice

All the mice were maintained in the central animal facility (CDP) of University Medical Center Groningen (UMCG) under standard conditions. All the experiments were approved by the Central Authority for Scientific Procedures on Animals (CCD) in Netherlands. For analyses of skin and liver, samples from naturally aged C577BL/6J mice were obtained from the mouse clinic for Cancer and Aging, University Medical Center Groningen (UMCG). For all other aging experiments, p16-3MR mice were used (Demaria et al., 2014). For experiment with hypoxia mimetics, 3,4 dihydroxybenzoic acid (Sigma-Aldrich, Cat# 37580) was dissolved in PBS and administered by daily I.P. Injection (10 mg/kg) for 7 consecutive days. Roxadustat (MedChem Express, Cat# HY-13426) was dissolved in vehicle (5% DMSO + 95% corn oil) and administered by i.p. injection (30 mg/kg) every other day for 3 times. All animals were bred in house. Aged mice were 24 months or older. Young control mice and doxo treated mice were between 3-6 months old (early adulthood). All mouse experiments were performed using mixed gender.

METHOD DETAILS

Cell morphology analysis

After 10 days in 1% or 5% O_2, cells were trypsinezed and brightfield images were acquired in a Countess™ II Automated Cell Counter (Thermo Fisher Scientific). Cell area of 50 cells per group was measured with ImageJ using pixels as scale.

EdU staining

Cells were re-plated on coverslips in a 24-well plate (1'*10^4-1,5*10^4 cells/well) and cultured for 24 hours in the presence of EdU (10 μM, Lumiprobe, Cat# 10540), fixed with 4% paraformaldehyde and stained as previously described (Hernandez-Segura et al., 2018a). In short, cells were incubated with 100mM Tris (pH7.6, 5min) and permeabilized using 0.1% Triton in PBS (10min). Cells were incubated with staining mix containing PBS, Cu(II)SO4 (2uM, Sigma-Aldrich cat# 209198), sulfo-Cy3-azide (4uM,Lumiprobe, Cat# D1330) and sodium-ascorbate (20mg/ml,Sigma-Aldrich, Cat#A4034). Afterward cells were washed with PBS, counterstained with DAPI by incubating the cells with 1ug/ml DAPI solution (Boster Biological Technology, Cat# AR1177) and mounted onto a glass slide using ProLong Gold Antifade Mountant (Invitrogen, Cat# P36934). Images were acquired at 100 times magnification (Leica) and number of EdU^+ cells were counted using the ImageJ Software. Images were cropped using Microsoft Power Point.

Senescence-associated β-galactosidase staining

Cells were re-plated on coverslips in a 24-well plate ($1*10^4$-$1,5*10^4$ cells/well) and stained as described previously (Hernandez-Segura et al., 2018a). In short, cells were fixed by incubation in 2% formaldehyde + 0.2% glutaraldehyde in PBS for 3 minutes. Then, cells were washed and incubated for 12-16 hours at 37 degrees in de dark, in freshly prepared staining solution containing 40mM citric acid/sodium phosphate buffer (pH 6.0), 5mM potassium ferrocyanide, 5mM potassium ferricyanide, 150mM Magnesium Chloride, 2mM Sodium Chloride and 20mg/ml X-gal (Cayman Chemical, Cat# 16495) in water. After staining, cells were washed with PBS and representative images were acquired using a microscope (EVOS). Then, nuclei were stained by incubating the cells with 1ug/ml DAPI solution (Boster Biological Technology, Cat# AR1177) for 20 min at room temperature in the dark. After 3 washes with PBS, cells were conserved in 70% glycerol and images were acquired at 100x magnification with a microscope (Leica). $Saβgal^+$ cells were counted using the ImageJ software. Images were cropped using Microsoft Power point.

Immunofluorescence

For cell culture staining, cells were re-plated on coverslips in a 24-well plate ($1*10^4$-$1,5*10^4$ cells/well). At the time point of staining, cells were washed with PBS, fixed for 15 min with 4% paraformaldehyde, washed with PBS and permeabilized for 15 min. with 0.1% Trition-100-X in PBS. Afterward, cells were washed in PBS and blocked using 10% Normal Goat Serum (Sanquin) for 45 min and incubated with primary antibody (gamma-H2A.X, 1:1000 dilution; Novus Biologicals, Cat# NB100-384) overnight at 4°C. Cells were incubated with secondary antibody (Thermo Fisher Scientific, Goat anti-Rabbit IgG, Alexa 488, Cat #R37116) washed with PBS and nuclei were stained using 1 μg/ml DAPI solution (Boster Biological Technology, Cat# AR1177) for 20 min

at room temperature in the dark. Coverslips were mounted using ProLong Gold Antifade Mountant (Thermo Fisher Scientific, Cat# P36934). Images were acquired at 100x magnification with a microscope (Leica). Number of foci per cell was quantified using ImageJ software. Images were cropped using Microsoft PowerPoint.

For human IL6 and p16 double staining, paraffin embedded renal sections from brain-dead organ donors prior to reperfusion were used. Tissue sections on glass slides were deparaffinized by incubation with xylenes (15 min), 100% ethanol (3 min), 96% ethanol (3 min), 70% ethanol (3 min) and water (5 min). For antigen retrieval, slides were boiled for 15 min in citrate buffer (pH 6) and cooled down to room temperature and washed. Then, tissue was blocked in 5% BSA in PBS for 1h at RT in a humid chamber. Slides were incubated with p16 antibody (Abcam, ab108349, 1:100 dilution) for 1h at RT in a humid chamber. After 3 washes with PBS, slides were incubated with secondary antibody (Thermo Fisher Scientific, Goat anti-Rabbit IgG, Alexa 488, Cat #R37116), 1h at RT, and washed 3 times with PBS. Then tissue was blocked in 5% Normal goat Serum and incubated with IL6 primary antibody (Abcam, ab6672, 1:100 dilution) at 4°C O/N in a humid chamber. The next day, tissues were washed with PBS, incubated with secondary antibody (Thermo Fisher Scientific, Goat anti-Rabbit IgG, Alexa 488, Cat# A-24124) and washed in PBS. Counterstaining was done using 1 μg/ml DAPI solution (Boster Biological Technology, Cat# AR1177) for 20 min at room temperature in the dark. Afterward, slides were washed, coverslip was mounted and sealed with nail polish. The paraffin embedded aged mouse renal sections were stained with phospho-S6 ribosomal protein (Ser235/236) (Cell signaling, Cat# 4858, 1:200 dilution) with the same protocol as above-mentioned. Image acquisition was performed with confocal microscope Leica TCS SP8 (Leica, Wetzlar, Germany). Images were cropped using Microsoft PowerPoint.

Real-time PCR

Total RNA was isolated using the Isolate II RNA Mini Kit (Bioline, Cat# BIO-52073). 125-500 ng of RNA was reverse transcribed into cDNA using a kit (Applied Biosystems, Cat# 4368813). qRT-PCR reactions were performed using the Universal Probe Library system (Roche) and a SensiFast Probe kit (Bioline, Cat# BIO-84020). The geometric mean of the expression levels of Actin and Tubulin was used to normalize the expression of CP values unless otherwise indicated. Every sample was analyzed in duplicate. List of primers and probes is provided in Table S1.

Protein sample preparation and enzyme-linked immunosorbent assays (ELISA)

To collect conditioned medium, cells were re-plated and incubated in serum free medium for 24 hours. The CM was centrifuged for 5min (300 *g*) to remove any cells or debris and stored in −80°C until use. For total protein lysates of mouse organs, tissues were snap frozen in liquid nitrogen immediately after collection, homogenized in liquid nitrogen using a mortar and pestle and immediately lysed in cold RIPA buffer (Abcam, Cat# ab156034) supplemented with proteinase and phosphatase inhibitors (Pierce, Cat# A32959). Then, samples were sonicated and spun down for 5 min (300 *g*) to remove any debris. Total protein levels were measured using a BCA protein assay kit (Pierce, Cat# 10741395). At the time of ELISA performance conditioned medium or tissue lysates were thawed on ice and equal amounts of total protein was analyzed according to manufacturer's protocol using the following kits: Human IL-6 duo-set (R&D Systems, Cat# DY206), Human CXCL1GRO-α (R&D Systems, Cat# DY275), a custom made multiplex human Magnetic Luminex Assay kit (R&D Systems) to detect protein levels of IL6, CXCL1, CXCL10, CCL5, CCL2, IL1α and IL1β, Mouse CXCL1/GRO-α (R&D systems, Cat# DY453) and Mouse IL6 (R&D systems, Cat #DY406).

Transwell migration assay

MDA231 breast cancer cells ($2*10^4$) were re-suspended in serum–free medium and seeded in a transwell insert (8 μm pore, Corning, Cat# 3422) with serum-free media collected from senescent cells in the outer chamber of a 24-well culture dish. Cells were cultured in a 5% O_2, 5% CO_2, 37°C incubator for 24 hours and cells remaining in the upper part of the transwell were removed using a cotton swap. Thereafter, cells migrated to the lower side of the transwell were fixed with 4% PFA and stained with 0.5% crystal violet/10% methanol solution. Images were acquired at 40X magnification with a microscope (Leica or EVOS). Number of migrated cells were analyzed using ImageJ software. Representative pictures were cropped using Microsoft PowerPoint.

Immunohistochemistry

Mouse kidney tissue sections on glass slides were deparaffinized by incubation with xylene (10 min), 100% ethanol (2*3 min), 96% ethanol (2*3 min), 70% ethanol (2* 3min) and water (2*5 min). For antigen retrieval, citrate buffer (pH 6) was pre-heated, slides were boiled for 10 min in warm citrate buffer, cooled down to room temperature and washed. Endogenous peroxidase activity was blocked by incubation with 1% H_2O_2 in methanol solution for 10 min. After washing with PBS, tissues were blocked by 10% Normal goat serum for 30 min. Slides were incubated with primary p21 antibody (Santa Cruz Biotechnology, Cat# Sc-471, 1:400 dilution) or IL6 antibody (Abcam, Cat# ab6672, 1:100 dilution) in a humid chamber, O/N at 4°C. The next day, slides were washed, incubated with secondary antibody (Vector laboratories, goat anti-rabbit\biotin, Cat# BA-1000) for 30 min at RT, washed and incubated with ABC/PO-Complex (Vector laboratories, Cat# PK-4000). Then, tissues were washed and incubated with freshly prepared DAB substrate (5 mL 70 mM DAB, 45 mL 0.05M Tris-HCL pH 7.8 and 5 μl 35% H_2O_2) and counterstained with hematoxylin. Slides were dehydrated and coverslip was mounted using Eukitt mounting reagent (Sigmaaldrich, Cat# 03989). Pictures were made using a microscope (Hamamatsu) and quantified using ImageJ software. Images were cropped using Microsoft PowerPoint. GL13 staining (Sentragor©) and evaluation were performed as previously described (see also Gorgoulis et al., 2019 and references therein). Tissue

sections were deparaffinized by incubation at 60°C and washing in Xylenes (15min). Sections were gradually rehydrated by subsequent incubation in 100%, 96%, 80%, 70% and 50% ethanol for 5 min each. Tissue sections were washed in TBS and endogenous hydrogen peroxidase activity was blocked by Ultravision Hydrogen Peroxide Block included in the Ultravision Quanto Detection System HRP DAB kit (Cat# TL125-Q-HD) according to manufacturer's protocol. Then, tissues were washed in TBS and Ethanol followed by incubation with the GL13 compound (Sentragor©) at RT. Staining reaction was monitored under a light microscope until detection of the signal (on average 5-8 min). Afterward, tissues were washed in ethanol, permeabilized by incubation with 0.5% triton (3 min) and incubated with anti-biotin antibody (1:500, Abcam,Cat# ab201341) for 60 min at 37°C. Tissues were washed in TBS and biotin antibody was detected using Ultravision Quanto Detection System HRP DAB kit (Cat# TL125-Q-HD) according to manufacturer's protocol. A coverslip was mounted onto tissue section with permanent mounting media Glycergel (DakoCytomation).

Immunoblot analysis

Protein lysates were obtained by scraping cells in cold RIPA buffer (Cat# ab156034, Abcam) supplemented with proteinase and phosphatase inhibitors (Cat# A32959, Pierce (TFS) on ice. Protein sample buffer was added to get a final concentration of 40 mM Tris-HCL, 1.9% SDS and 3.1% β-mercaptoethanol and 6.3% glycerol and samples were boiled for 5 min at 95°C. Equal amounts of sample was loaded on an SDS-PAGE gel (bis-acrylamide 29:1, Bio-Rad, Cat# 1610146) and blotted onto a 0.2 μm nitrocellulose membrane (Bio-Rad, Cat# 162-0112). Immunodetection was performed as recommended by the manufacturers of the following antibodies: Phospho-S6 Ribosomal Protein (Ser235/236) (Cell signaling, Cat# 4858), S6 Ribosomal Protein (Cell signaling, Cat# 2217), Phospho-p70 S6 Kinase (Thr389) (Cell signaling, Cat #9205), p70 S6 Kinase (Cell signaling, Cat #9202), Phospho-AMPKα (Thr172) (Cell signaling, Cat #2531), Phospho-mTOR (Ser2448) (Cell signaling, Cat# 2971), AMPK1/2α (Santa Cruz Biotechnology, Cat# sc-74461), HIF1α (BD Biosciences, Cat# 610958), Actin (MP Biomedicals, Cat# 06891001) and Vinculin (Sigma-Aldrich, Cat# V9131). ECL Prime western blotting detection reagent (GE Healthcare, Cat# RPN2232,) was used according to manufacturer's guidelines for detection and the signal was measured using an ImageQuant LAS 4000 biomolecular imager (GE Healthcare). Densitometry was performed using ImageJ Software and values for protein of interest were normalized to vinculin levels or actin levels which served as loading controls.

Detection of cell surface-bound IL1α using FACS

A fluorescein-conjugated antibody (R&D Systems, Cat# FAB200F) was used to detect cell surface-bound IL1α. Measurement and analysis was done by flow cytometry using a BD Canto II flow cytometer and software, as described previously (Laberge et al., 2015). In short, 3 × 105 cells were washed with PBS, detached from the culture flask using accutase (Sigma-Aldrich, Cat# A6964), and collected by centrifugation at 300 x g. Washing of the cell pellets with ice-cold PBS containing 0.5% BSA (0.5%BSA/PBS) was followed by blocking with 2% FBS in 0.5%BSA/PBS. Incubation with the fluorescein-conjugated antibody (per 105 cells 10 μl was added) was performed cold and in the dark. Following two washes with 0.5%BSA/PBS, the cells per suspended in 0.5% BSA/PBS for analysis on the flow cytometer.

Generation of lentiviral NF-kB reporter vector

Plasmid pGL4.32 [Luc2P/NF-κB-RE/Hygro] (Promega, Cat# 8491) was used as template DNA in a PCR for obtaining the NF-kB response element under the control of the minimal promotor Luc2P. For the PCR reaction the following primers were used: Forward: 5′-aaaaatcgatggcctaactggcggtac-3′,Reverse: 5′aaaaaggatcccgactctagagtcgcggcc-3′ in combination with Phusion High Fidelity DNA polymerase (New England Biolabs, Cat# E0553S,). The PCR product was purified from gel, cut with ClaI (Roche, Cat# 10656291001) and BamHI- HF (NEB, Cat# R3136s) and ligated into the backbone vector pLenti[CMV/GFP/Hygro] (656-4), a gift from Eric Campeau & Paul Kaufman (Addgene plasmid #17446). The cut backbone vector was treated with Antarctic Phosphatase (NEB, Cat# M0289S) before ligation. T4 DNA ligase (NEB, Cat# M0202S) was used in the ligation reaction. All enzymes were used according to manufacturer's manual. The ligation reaction products were transformed into NEB stable Competent *E. coli* (High Efficiency, NEB, Cat# c3040h) and grown overnight at 37°C on LB plates supplemented with 50 μg/ml Ampicillin. A colony PCR was performed to check for positive clones. Single positive clones were grown overnight in liquid LB supplemented with Ampicillin at 37°C to be midiprepped using a PureLink® HiPure Plasmid Midiprep Kit (Invitrogen, Cat# K210005). This newly generated lentiviral NF-κB-reporter vector (pLenti-NF-κB-RE-minP-LUC-EGFP-hygro) was sent to GATC/Eurofins for sequencing and verification of the Luc2P/NF-κB-RE insert.

Generation of lentiviral particles

293FT cells were seeded in a 10 cm Petri dish at $5*10^6$ cells. Next day, cells were transfected with the ViraPower plasmid mix (Invitrogen, Cat# K4970-00) together with the lentiviral vectors using PolyFect transfection reagent (QIAGEN, Cat# 301105) overnight. The medium with transfection mix was replaced for normal growth medium without antibiotics, collected after 48 hours and concentrated using Peg-It Virus precipitation solution (System Biosciences, Cat# LV810A-1) according to the manufacturer's manual.

Lentivirus transduction

Lentiviral particles harboring either an shRNAs against Hif-1alpha (MISSION shRNA libray, Sigma Aldrich, TRCN0000003810, Sequence: GTGATGAAAGAATTACCGAAT), the lentiviral NF-kB-luc plasmid prepared as described above, or a vector for

AMPK overexpression (Addgene, Cat# 74446) were made in house. Cells were seeded in a 6 well plate and the next day infected with the lentiviral particles (1:50-1:100 dilution in complete medium) for 24 hours in the presence of Polybrene (6 μg/ml; Santa Cruz Biotechnology, Cat# sc-134220,) to enhance transduction efficiency. Cells were washed and refreshed with complete medium on day 2. Selection was started at day 3 (Hif-1α, NF-kB reporter,AMPK and shTSC1: puromycin, 2 μg/ml, Sigma, Cat# P8833; RAS: G418, 200 μg/ml, Thermo Fisher Scientific, Cat# 11811031). For Hif-1α knockdown, wi38 cells transduced with pLKO.1-scrambled lentiviral particles served as control cells.

QUANTIFICATION AND STATISTICAL ANALYSIS

Details about the statistical analysis for each figure are provided in the figure legends. Significance is indicated as as follows: *$p < 0.05$, **$p < 0.01$, ***$p < 0.001$, NS, Not-significant.

Microsoft Excel was used for the statistical analyses.